

# Service Restoration in Low Voltage MicroGrids with Plugged-in Electric Vehicles

C. Gouveia, C. L. Moreira\*, J. A. Peças Lopes, D. Varajão, R. Esteves Araújo

INESC Porto and Faculdade de Engenharia da Universidade do Porto, Rua Dr. Roberto Frias 378,  
4200-465 Porto, Portugal

\* Corresponding author

Tel.: +351222094210

Fax: +351222094150

E-mail address: [carlos.moreira@inescporto.pt](mailto:carlos.moreira@inescporto.pt)

---

## *Abstract*

The development of the Microgrid concept endows distribution networks with increased reliability and resilience and offers the adequate management and control solution for massive deployment of microgeneration and Electric Vehicles. Within a Microgrid, local generation can be exploited to launch a local restoration procedure following a blackout. Electric Vehicles are flexible resources that can also be actively included in the restoration procedure, thus contributing to improve Microgrid operating conditions. The feasibility of Microgrid service restoration, including the active participation of Electric Vehicles, is demonstrated in this work through extensive numerical simulation and experimentally in a laboratorial setup.

*Keywords:* Black Start, electric vehicles, energy storage, frequency control, microgrid, voltage unbalance.

---

## **1. Introduction**

Meeting reliability requirements in electric power distribution systems characterized by a high penetration of Distributed Energy Resources (DER), load variability and massification of Plugged-in Electric Vehicles (EV) is becoming a challenging task [1]. In order to ensure reliability, security and quality of supply, innovative decentralized control architectures should be developed at the distribution level, aiming a higher system observability and controllability, while assuring better control and management

performances. The materialization of this scenario is in line with the smart grid development, in which the MicroGrid (MG) plays a central role [1], [2].

The MG is a flexible cell of the electric power system, incorporating local generation based on renewable energy sources and low carbon technologies for combined heat and power applications, storage devices and loads [3]. The MG resources can be coordinated by a local management and control system in order to properly support the operation of the Low Voltage (LV) network and control the power flow between the MG and the upstream Medium Voltage (MV) network in coordination with the distribution system operator requirements [3]-[5].

MG operation can be divided in two distinct modes: normal operation mode and emergency operation mode. The normal operation mode is considered whenever the MG is interconnected to the MV network. However, when major disturbances occur in the main grid, the MG can be operated autonomously – emergency operation mode – by exploiting storage, locally available generation sources, as well as the flexibility of some controllable loads [2]-[4]. In case a general blackout occurs, decentralized self-healing strategies can also be developed at the MG level in order to restore the service to LV consumers [6]-[8]. This new distribution network operation philosophy increases reliability and continuity of supply at the distribution level and improves system resilience against component failures and natural disasters.

The occurrence of general blackouts is a rare event but has severe economic and social impacts, as a consequence of the long restoration times resulting from complex restoration procedures [9]-[11]. The unique characteristics of each electric power system preclude the definition of general restoration plans. For each step of the restoration procedure, system operators have to deal with a large number of system variables in order to maintain system stability and avoid a new system collapse [11].

When compared to conventional power system restoration, the MG Black Start (BS) procedure will benefit from a considerable problem size reduction. However, maintaining stability conditions in the MG requires specific voltage and frequency regulation strategies, exploiting the coordination between MG energy storage devices, Microsources (MS) generation capacity and load flexibility [4]-[6].

Additionally, the EV parked and connected to the grid for charging purposes, can be regarded as highly flexible loads, which can also provide additional storage capacity. The adoption of innovative control strategies at the EV charging interfaces have been shown to improve the frequency regulation capability and increase MG resilience during autonomous operation [12]-[14]. Hence, the participation of EV in the MG restoration procedure has the potential to enhance system resilience by contributing to avoid large frequency excursions resulting from loads or MS power variations.

This paper provides an overview of the MG restoration strategy, which is then extended to actively integrate the participation of EV. The effectiveness of the strategy proposed for the integration of EV within the MG restoration procedure is tested through extensive numerical simulation in order to validate the rules and conditions involved in the restoration procedure. Complementarily, a MG laboratorial setup was developed in order to experimentally demonstrate the feasibility of the proposed approach. During MG restoration voltage unbalance issues resulting from single phase loads and generation are also addressed, involving the exploitation of active voltage balancing strategies to mitigate the associated phenomena.

## **2. MG Emergency Management and Control: A Review**

As shown in Fig. 1, the MG management and control architecture is headed by the MG Central Controller (MGCC), which is installed at the MV/LV substation. The MGCC concentrates the high level decision making for the technical management of the

MG, including a software module dedicated to the MG restoration procedure [3],[4]-[6]. The lower control layer consists of a network of local controllers with local intelligence and bidirectional communication capabilities, which ensure the flow of information with the MGCC. Considering the different MG elements, three types of local controllers are considered, namely: the load controller (LC), the MS controller (MC) and the EV controller (VC) [4], [12], [13]. The VC enables the control of the EV battery charging and the exchange of information between the EV and the MGCC [12]-[14].

During the emergency operating mode, MG stability relies on the effectiveness of voltage and frequency regulation strategies, which have to be compatible with the MS and energy storage units operational characteristics [4]-[5]. Additionally, when operating isolated from the main grid, the MG is more sensitive to voltage unbalance problems caused by the uneven connection of single-phase loads and MS that could be further accentuated by the connection of single-phase EV charging interfaces [12], [14]. Voltage unbalance is a major drawback regarding the operation of three-phase loads (such as motor loads) decreasing its efficiency and lifetime. In order to maintain adequate voltage quality levels, active voltage compensation strategies have also been developed that eliminate the unwanted negative and zero sequence voltages components [15]-[17].

#### *A. MG Emergency Control Strategies*

In the moments subsequent to MG islanding or in the initial phases of the restoration procedure the MG requires some form of energy buffering in order to ensure power balance between generation and load. The MG power balancing is ensured by storage units capable of providing fast power compensation, such as flywheels or deep cycle battery banks. In order to ensure MG survival in the moments subsequent to islanding, an energy storage device (MG main storage in Fig. 1) is usually connected to the

MV/LV substation. The storage unit is coupled to the MG through a Voltage Source Inverter (VSI) that operates as a grid forming unit and provides MG voltage and frequency reference.

The MG can be operated with a single VSI in a Single Master Operation (SMO) mode or with more than one VSI following a Multi-Master Operation (MMO) strategy. In order to improve the security of operation during the MG restoration procedure, an MMO strategy is usually adopted [6], [7]. In this case, some of the controllable MS, such as Single Shaft Micro-Turbines (SSMT), will be equipped with a dedicated DC link storage unit that enables the generating unit autonomous re-start. Under these conditions, SSMT will be able to actively participate in the MG BS, operating temporarily as additional grid forming units [6], [7].

The control strategy usually followed at VSI naturally provides primary frequency regulation. The VSI are locally controlled through droop functions, reacting autonomously to grid operating conditions, as in (1), where  $\omega_0$  and  $V_0$  are the idle values of the angular frequency,  $\omega$ , and voltage,  $V$ ,  $k_P$  and  $k_Q$  are the droop slopes (positive quantities),  $P_i$  and  $Q_i$  are the active and reactive power output at the idle frequency and voltage and  $\Delta P$  and  $\Delta Q$  are the inverter active and reactive power output, required to ensure power balance in a MG. Similarly, in MMO mode, both the MG central storage unit and the MS dedicated storage units will contribute to the MG primary frequency regulation, injecting power according to their capacity and droop characteristics, as in (2), where the variables are referred to unit  $i$  and  $\omega'$  is the MG frequency after the islanding [4], [5]. The sum of the active power injected by all the storage units will be equal to the total power unbalance  $\Delta P$ .

The implementation of secondary frequency control is also required to correct the MG permanent frequency deviation, resulting from the use of a proportional control at

VSI. Fig. 2 shows the centralized secondary control algorithm adopted in this research. The algorithm is implemented at the MGCC and performs the MS power dispatch if the MG frequency deviation exceeds a pre-defined limit ( $\Delta\omega_{min}$ ). The MG power unbalance ( $\Delta P$ ) is determined based on the power injected by the MG main storage unit ( $P_{VSI}$ ) connected to the MV/LV substation. When the frequency deviation exceeds the pre-defined limit ( $\Delta\omega_{min}$ ), the algorithm determines new idle values for the angular frequency of the MS droop characteristics ( $\omega_0$ ), in order to obtain the desired power adjustment ( $\Delta P_{MSi}$ ). The contribution of each controllable MS will be defined through a participation factor ( $f_{pi}$ ), which is determined (for unit  $i$ ) by the ratio between its reserve and the total controllable MS reserve. The resulting set-points are then sent from the MGCC to local MC.

#### *B. MG Unbalanced Operation during Emergency Conditions*

As it was previously mentioned, the presence of single phase loads (including EV charging interfaces) and MS affect the MG voltage balance. In particular, when operating autonomously, the MG short circuit power is substantially reduced, thus increasing the existing voltage unbalance problems. The implementation of additional control loops at the MS coupling inverters contributes to mitigate the MG voltage unbalance during autonomous operation [12], [15]-[17]. The control strategies proposed in [15] and [16] were designed for three-phase unbalanced systems in order to compensate negative sequence voltage components at the MS terminals and at the point of common coupling, respectively. However, the LV network is usually a three-phase four wire system, having also a zero sequence component when operated under unbalanced load conditions. In [17] the authors propose a compensation method for three-phase four wire MG applications, which is able to compensate both negative and zero sequence voltage components through the use of a four-leg shunt inverter.

The four-leg shunt VSI proposed in [17] was adopted in this research in order to balance the MG voltages during the restoration procedure. The VSI with the additional voltage balancing mechanism is able to provide three independent output reference voltages, regardless of the MG loading conditions. The main building block of the VSI controller is represented in Fig. 3. The voltage compensation control loops are implemented in the stationary reference frame  $(\alpha, \beta, 0)$ . The frequency and magnitude of the desired output voltages are determined through P- $\omega$  and Q-V droops. Then, the voltage reference signals in the stationary reference frame  $(V_a^*, V_\beta^*, V_0^*)$  are compared with the actual inverter terminal voltage. The resulting error is injected in a voltage-current control loop, constituted by an inner current loop and an outer load voltage control loop. The voltage controller consists in three proportional-integral resonant controllers  $(G^+(s), G^-(s), G^0(s))$ . The inner current control loop consisting in a proportional controller will then determine the inverter output voltage  $(V_a^*, V_b^*, V_c^*)$ .

### C. Integration of EV on the MG Hierarchical Control

The load controllability and distributed storage capacity provided by EV (when parked and connected to the LV network) can be properly exploited for improving the MG frequency regulation capacity. In [12], [13] the authors propose an active power/frequency (P- $f$ ) droop control strategy to be implemented at the EV coupling inverter, where the EV will autonomously adapt its power output based on the MG frequency. According to the EV P- $f$  droop represented in Fig. 4 b), when a disturbance occurs and the frequency drops below the dead-band minimum, the EV reduces its power consumption. For large underfrequency disturbances, greater than the zero-crossing frequency ( $f_0$ ), the EV batteries will discharge – thus providing the Vehicle to Grid (V2G) functionality. When the MG frequency increases to values higher than the dead-band maximum, the EV can also increase its power consumption. When the MG

frequency becomes out of the droop frequency range, the EV battery will inject/absorb a fixed power, which can also be defined.

In emergency operating conditions, the MGCC can remotely control the EV  $P$ - $f$  droop parameters (see Fig. 4 a)), such as the nominal charging power ( $P_{\text{rated}}$ ) for nominal frequency, the zero-crossing frequency ( $f_0$ ) in case there is the need of using the V2G capability and possibly the frequency ( $f_{\text{min}}$  and  $f_{\text{max}}$ ) and power ( $P_{\text{min}}$  and  $P_{\text{max}}$ ) limits.

### **3. The Role of EV in the MG Restoration Procedure**

During the MG restoration phase EV can be exploited as grid supporting units in order to take advantage of their storage capacity and charging flexibility. Similarly to what has been demonstrated for the MG islanding procedure, the EV can improve the MG frequency regulation capacity, supporting the frequency disturbances resultant from the reconnection of load and generation, and other transients that might occur during the restoration procedure. However, in order to provide support to the MG during the initial stages of the restoration procedure, the EV should be synchronized to the grid with a zero power set-point, as shown in Fig. 4. As a result of the modified  $P$ - $f$  droop characteristic to be used in the initial phase of the MG restoration procedure and whenever the frequency remains within the frequency dead-band, the EV will not exchange power with the MG. Afterwards, when loads and MS are gradually reconnected, the EV will inject or absorb power to support MG power balancing. Consequently it contributes to reduce MG frequency excursions and the power solicited to the main energy storage unit.

The MG restoration procedure will be triggered by the MGCC when a general or local blackout occurs or when the MV network is not able to restore MG operation after a pre-defined time interval. Similarly to conventional power systems, the MG

restoration procedure consists in a sequence of actions to be checked and performed by MG local controllers in coordination with the MGCC. The procedure should be fully automatic without requiring the intervention of distribution network operators. In order to perform service restoration at the MG level, it is assumed that the MG is equipped with:

- MS with black start capability, such as SSMT, capable of communicating to the MGCC their generation availability and operational status.
- LV switches to disconnect the MG feeders, loads and MS in case a generalized blackout occurs.
- Communication infrastructure powered by dedicated auxiliary power units, in order to ensure the communication between the MGCC and the local controllers.
- Adequate protection equipment in order to protect MS and the LV grid from the fault currents and to isolate the faulted area.

Following the MG restoration strategy presented in [6] and the proposed EV control strategy the overall procedure can be organized in the following sequence of events:

1. MG status determination. The MGCC evaluates the network status both upstream and downstream:
  - a. Upstream network status – the MGCC only launches the restoration procedure if there isn't any alternative to reconnect the MG to the main grid. Therefore, the MGCC waits for the distribution system operator authorization in order to activate the BS procedure.
  - b. Downstream network status – the MGCC evaluates the LV network status, analyzing switches status and alarms, in order to check the existence of local faults or equipment failures. At this stage the MGCC

also evaluates the available generation and active load resources, in order to ensure the successful MG service restoration. Historical data resulting from the MG operation can provide information about the priority loads to be restored.

2. MG preparation in order to start the restoration procedure. The MGCC sends a signal to the local controllers (MC, LC and VC) in order to ensure the disconnection of loads, MS and EV. Then, MS with BS capability can be restarted to power some local loads. This procedure ensures that the MS with storage capacity providing back power to their local loads are not energizing larger parts of the LV network. As it was previously stated, the controllable MS coupling inverter is controlled as VSI with droop characteristics. In order to maintain the frequency close to nominal values, the idle power and frequency values of ( $P_i$  and  $\omega_{0i}$ ) of the MS droop characteristic have to be adequately parameterized.
3. LV grid energization, through the connection of the MG main storage unit installed at the MV/LV substation and by closing the substation LV feeder switches. The connection of the MG main storage unit in no load/generation conditions ensures the MG operation with nominal frequency and voltage.
4. Synchronization of the running MS to the MG. The synchronization is enabled by the MGCC, being the necessary conditions – such as phase sequence, frequency and voltage differences (both in phase and amplitude) checked by the MC, through synchro-check relays.
5. Reconnection of EV to the MG. The EV chargers are connected to the LV network with initial zero consumption (see Fig. 4), causing as minimum impact as possible.

6. Coordinated reconnection of loads and non-controllable MS, considering the available storage capacity and local generation, in order to avoid large frequency and voltage deviations during load and non-controllable generation connection. The secondary frequency control scheme presented in Fig. 2 will correct frequency deviations, ensuring that the frequency remains close to nominal values. However, since the EV are participating in the MG frequency regulation it will be necessary to update the MG power unbalance ( $\Delta P$ ) based on the power injected by the MG main storage unit connected to the MV/LV substation ( $P_{VSI}$ ) and by the EV ( $P_{EV}$ ). After the reconnection of all the MG loads, if there is sufficient reserve capacity, the MGCC can gradually increase the EV charging power for nominal frequency ( $P_{rated}$ ).
7. MG synchronization with the main grid after service restoration at the MV network. The MGCC should receive a confirmation from the distribution network operator to start the synchronization with the upstream network. The synchronous conditions are checked locally through a synchro-check relay.

#### **4. Validation of the MG Restoration Procedure with EV**

The LV test network represented in Fig. 5 was adopted in order to demonstrate the benefits of the EV participation on the MG primary frequency regulation. The LV network is operated under unbalanced conditions due to the connection of single-phase loads and MS. Two SSMT with local storage capacity are connected to nodes 25 and 75. The MG main storage unit which is connected to the LV bus of the MV/LV substation has a maximum power capacity of 100kW. It was assumed that the storage unit has sufficient capacity to ensure the MG stability during the restoration procedure. The VSI connected to the MG main storage unit and to the SSMT will inject or absorb their maximum admissible power for a maximum frequency deviation of  $\pm 1$  Hz. The

simulation scenario is summarized in Table I regarding the loads, MS production and EV rated power.

The MG system was modeled in a *Matlab/Simulink* environment through the use of the *SymPowerSystems* toolbox and user-defined models. The simulation platform allows analyzing MG dynamic behavior considering the control strategies discussed in section 2 and 3. When analyzing the MG dynamic behavior, inverters were modeled using an average (RMS) model, neglecting fast switching transients, harmonics and losses. This is a general procedure adopted by several authors when dealing with power electronic interfaces in stability studies [4], [12], [18]. A detailed description of the adopted dynamic models of MS, storage devices, EV chargers and power electronic interfaces can be found in [12], [18].

Regarding the simulation of the MG restoration procedure, it was assumed that when the simulation starts the MG is already disconnected from the main grid and it is energized by the VSI connected to the MG main storage unit. At this phase, all MG loads, EV and MS are still disconnected. The complete restoration procedure is described in Table II. The time instances of the restoration events were chosen based on a continuous evaluation of the MG frequency response to the restoration events and taking into account the reaction time of the primary and secondary frequency control. The rationale for the choice of the time instances is directly related to the need of avoiding large frequency disturbances, therefore requiring system stabilization after each step of the restoration procedure.

Before synchronizing to the LV grid, it is assumed that SSMT successfully restart and feed some local loads (Fig. 6). The VSI droop parameters, namely  $P_i$  and  $\omega_{0i}$  were able to maintain the frequency close to nominal values. After reenergizing the MG, the MGCC initiates the synchronization of the SSMT installed at nodes 25 and 75. Fig. 6 a)

shows the MG and SSMT frequency during the synchronization procedure. At  $t=3$ s the local synchro-check relays introduces a small frequency change in the SSMT inverter in order to facilitate the synchronization process. The synchronization conditions are verified at  $t=4$  s and the SSMT in node 25 successfully connects to the MG. At  $t=7$ s the MGCC enables the synchronization of the SSMT in node 75 which reconnects successfully to the MG at  $t=7.7$ s. The active power response of the MG storage unit and SSMT during the synchronization procedure is shown in Fig. 6 b). After the reconnection transient, the MG storage unit coupled to a VSI and the SSMT share the MG load. Since the MG frequency deviation is smaller than the minimum frequency deviation which triggers the secondary control (a 0.05 Hz dead-band was considered in the simulations), no power adjustment was defined by the MGCC.

#### *A. Analyzing the benefits of EV participation on the MG frequency regulation*

In order to evaluate the effectiveness of the EV participation in the MG frequency regulation, two cases were considered: a base case where the EV do not participate in the restoration procedure, being treated as conventional loads, and a second case where the EV are controlled through a  $P-f$  droop characteristic. In the second case, the EV are connected to the MG with a zero power set-point after the SSMT synchronization, at  $t=16$  s of the simulation time.

Fig. 7 compares the MG frequency response during the service restoration time for both cases. The active participation of EV in the frequency regulation reduces the frequency deviation caused by the reconnection of loads ( $t=20$ s and  $t=65$ s) and non-controllable MS ( $t=45$ s). As represented in Fig. 8, the EV inject power during the reconnection of loads and increase their power consumption during the reconnection of the micro-wind turbines and PV panels. According to the EV frequency droop characteristic, the participation of EV in frequency regulation becomes more significant

for large frequency disturbances. However, as shown in Fig. 9, when considering the V2G operation mode there is a reduction of the active power required from the MG main storage unit.

When the frequency stabilizes ( $t=75s$ ) and since the MG had enough reserve capacity, the P- $f$  droop parameter  $P_{rated}$  is increased gradually, in order to allow EV to charge their batteries.

### *B. Analyzing the MG unbalanced operating conditions*

In order to study the benefits of adopting voltage balancing mechanisms, the four-leg inverter with the voltage balancing mechanism described in section 2.2 was considered. Voltage unbalance was measured by the Voltage Unbalance Factor (VUF) as described in EN50160 standard [19], regarding the voltage negative sequence component ( $V_2/V_1$ ) and the zero sequence voltage unbalance factor ( $V_0/V_1$ ). Fig. 10 and Fig. 11 show the VUF and the three-phase voltages at the VSI terminals, considering the four-leg inverter with the voltage unbalance compensation loop (on the left) and a three-leg inverter (on the right). In both cases, voltage unbalance is within the 2% admissible limit [19]. However, the balancing unit is able to eliminate the voltage unbalance at the VSI terminals, balancing the three-phase voltages supplied by the VSI. As a consequence, the voltage unbalance is also reduced in the other MG nodes. Fig. 12 and Fig. 13 show the voltage unbalance and the three phase voltages at node 71 (which is located at the end of a feeder). As shown in Fig. 12, both negative and zero sequence voltage unbalance were reduced, as a consequence of the voltage compensation at the VSI terminals.

## **5. Experimental Demonstration of the EV Role in the MG Restoration**

A smart grid laboratorial infrastructure dedicated to the development of active distribution networks, based on the MG concept, was developed at INESC Porto.

Similarly to the MG architecture, the laboratory architecture can be divided in the power infrastructure complemented by a communication and information layer, constituting the MG management and control functionalities.

The laboratory includes renewable based microgeneration (3 kW micro-wind turbine emulator and 6 kWp photovoltaic panels), storage (25 kWh capacity Flooded Lead-Acid (FLA) battery banks and 128 Lithium battery cells for the EV charging prototype), a 54 kW resistive load bank and LV cables emulator, thus enabling the implementation of a three-phase four wire MG system [20]. The micro-wind turbine emulator is connected to a commercially available *SMA Windy Boy 3000* single-phase inverter and the photovoltaic strings are connected to three single-phase *SMA Sunny Boy 1700* inverters.

In order to enable the autonomous operation of the MG, a three-phase group of commercially available VSI – three *SMA Sunny Island 5048* – is coupled to the FLA battery bank. The *Sunny Island* inverters are mainly used for the electrification of remote areas, being able to operate autonomously in isolated systems, managing storage and local generation (renewable based and/or small backup generators). The inverters provide both frequency and voltage regulation to the islanded system. Primary frequency control is provided by an internal  $P-\omega$  droop characteristic, including also an additional secondary frequency control strategy, which allows restoring the grid frequency to the nominal value. However, when the batteries are charged and there is an excess of power generation (regarding the MG load), these inverters automatically increase the MG frequency, activating a built-in Automatic Frequency Control (AFC) functionality. This function avoids batteries overcharging by gradually increasing the inverter frequency, thus forcing the gradual reduction of the microgeneration power output, or even its disconnection [21].

The laboratory infrastructure incorporates several commercial solutions for microgeneration and energy storage applications. The main objective is to develop new control strategies, which are able to coordinate the MG resources considering the functionalities and limitations of currently available commercial solutions. However, in order to actively incorporate the proposed EV charging strategies within the experimental MG, a bi-directional EV charger prototype was also developed, being described in the next sub-section. As it will be shown in sub-section 5.C, the prototype was fully integrated and operates in coordination with the commercial solutions.

#### *A. EV bidirectional charger prototype*

The EV charger pre-prototype consists of an isolated bidirectional AC-DC converter, coupled to a lithium-ion battery bank, as described in [22]. The charger can be divided in two stages with independent control schemes, as represented in Fig. 14. The first one is a grid tied Full-Bridge (FB) inverter that controls the power flow between the DC bus and the LV grid. The other stage is a Dual Active Bridge (DAB) that regulates the current in the batteries and assures galvanic isolation between the grid and the battery pack. The FB inverter regulates the DC bus voltage ( $V_{DC1}$ ) to 400V, in order to ensure adequate supply to the DAB input stage. The inverter is controlled with a PQ strategy, using a proportional-integrative controller implemented in a synchronous reference frame with additional harmonic compensation loop to assure high power quality. The grid frequency and voltage phase are estimated using a PLL algorithm, based on the grid voltage and current measurement ( $v_{ac}$  and  $i_s$ ) [23], [24].

The DAB consists of two full bridges connected by means of a high-frequency transformer. This type of DC-DC converter presents excellent characteristics, such as: galvanic isolation, bidirectional power transfer, high power density, high efficiency, very low output current ripple and wide output voltage operation range [25]. The

converter is controlled in terms of the active power flowing to the battery pack, which is handled by the phase-shift between voltages of both bridges. The active power flow between the DC-DC converter and the batteries is defined based on the Battery Management System (BMS) and EV frequency droop characteristic, which can set the reference power ( $P_{ref}$ ) within a limit of  $\pm 3680W$ . In normal grid operating conditions, the BMS algorithm charges the batteries based on constant current-constant voltage charging method. However, during grid disturbances the EV frequency droop will determine a new reference charging power in order to reduce the MG power balancing. In order to ensure adequate management of the battery pack, the charging rate defined by the frequency droop characteristic may become limited by the BMS, if the battery pack is not able to accommodate the reference power.

Fig. 15 shows the developed EV charger prototype. The bidirectional power stage was mounted on a layered architecture. At the top it is possible to observe the control board, which was implemented using a Digital Signal Processor (DSP) with high-calculation capability. A CAN interface was used to communicate with the commercial BMS. The full-bridge IGBT modules, DC bus capacitor bank and the isolated voltage and current transducers were implemented at the bottom PCB. At the middle layer, high performance IGBT drivers were mounted to ensure proper and safe operation of the switching devices operating at 30 kHz.

### *B. Laboratorial Setup*

The participation of EV on the MG primary frequency regulation during the restoration stage was tested experimentally, considering the test system depicted in Fig. 16. The experimental set-up consists in a LV grid with two nodes: the first representing the MV/LV substation and a second node at the end of the feeder, emulated through a LV cable simulator ( $0.6 \Omega$  resistors per phase and neutral conductor). The MG elements

are connected in node 2, namely: the EV bidirectional charger prototype, a 27 kW controllable load bank, a variable speed 3 kW micro-wind turbine emulator and the PV panels coupled to *Windy Boy* and *Sunny Boy* inverters, respectively. The three-phase group of *Sunny Island 5048* inverters is connected to node 1. In the experimental setup, no additional secondary frequency control scheme was considered besides the previously mentioned *Sunny Island* built-in frequency control, since only renewable based generation was considered.

### C. Experimental Results

In order to experimentally test the EV grid support functionality during MG service restoration, the experimental system of Fig. 16 was energized by the *Sunny Island 5048* inverters. Then, the EV charger prototype was synchronized to the islanded system. As proposed in Section 3, in order to support the MG rebuilding phase, the EV droop control was parameterized with a zero power set-point, so it could inject (positive value) or absorb power (negative value) according to the frequency deviation.

Fig. 17 shows the first 20s of the experiment, where at  $t=4.6$  s a 6.7 kW three-phase resistive load was connected. As shown in Fig. 18, the increase of the MG load caused the frequency to drop to 49.08 Hz. Since the frequency dropped below the frequency droop dead-band, the EV started to inject power into the grid, reaching a maximum of 2.7 kW. After stabilizing the MG frequency, at  $t=43.4$  s the micro-wind turbine emulator starts to inject power into the grid reaching approximately 2 kW, followed by the connection of the PV panels, which starts to inject power at  $t=58$  s (see Fig. 19). Since the load is still higher than the production, the battery bank coupled to the *Sunny Island* inverters continues to supply the remaining power consumption, maintaining frequency at 50 Hz.

In order to show the EV capacity of increasing its charging rate, the load is disconnected at  $t=127.2$  s, causing an excess of power generation regarding the MG load, which is absorbed by the *Sunny Island* inverters. However, as shown in Fig. 20, as the batteries became charged, the MG frequency increased reaching a maximum of 50.6 Hz. Considering the EV  $P$ - $f$  droop characteristic, the EV bi-directional charger increased its power consumption to approximately 1.8 kW. Finally, when the load is reconnected at  $t=199$  s, the *Sunny Island* inverters secondary control corrects the frequency deviation to 50 Hz.

## **6. Conclusions**

This paper provides an overview of the development of self-healing strategies, thus endowing MG with black start capability. The development of these strategies has a strong focus on the active integration of EV, given its control flexibility either as a load or as a generator through the V2G functionality. Extensive dynamic simulations demonstrate that the integration of EV in the MG restoration procedure positively contributes to increase the MG resilience. The EV active frequency regulation scheme supports the reconnection of the loads and MS, while reducing MG frequency deviations as well as the solicitation from the main storage system. Following the MG experimental setup similar results were obtained, thus demonstrating the feasibility and benefits resulting from the active integration of EV in MG restoration procedures. The obtained results have also shown the effectiveness of additional voltage balancing strategies in reducing the unwanted negative and zero sequence voltage components in the MG nodes, providing significant improvements in terms of voltage quality.

## **7. Acknowledgments**

This work is funded by the ERDF – European Regional Development Fund through the COMPETE Program (operational program for competitiveness) and by National

Funds through the FCT – Fundação para a Ciência e a Tecnologia (Portuguese Foundation for Science and Technology) within project Microgrids+EV: Identification of Control and Management Strategies for Microgrids with Plugged-in Electric Vehicles, PTDC/EEA-EEL/103546/2008-(FCOMP-01-0124-FEDER-009866).

## 8. References

- [1] K. Moslehi, R. Kumar, "A Reliability Perspective of the Smart Grid," *IEEE Transactions on Smart Grid*, vol.1, no.1, pp.57-64, June 2010.
- [2] R.H. Lasseter, "Smart Distribution: Coupled Microgrids," *Proceedings of the IEEE*, vol.99, no.6, Pp.1074-1082, June 2011.
- [3] B. Lasseter, "Microgrids [distributed power generation]," *IEEE Power Engineering Society Winter Meeting 2001*, vol.1, pp.146-149 vol.1, 28 Jan-1 Feb 2001.
- [4] J.A.P. Lopes, C.L. Moreira, A.G. Madureira, "Defining control strategies for MicroGrids islanded operation". *IEEE Transactions on Power Systems*, vol.21, no.2, pp. 916- 924, May 2006.
- [5] J.M. Guerrero, J.C. Vasquez, J. Matas, L.G. de Vicuna, M. Castilla, "Hierarchical Control of Droop-Controlled AC and DC Microgrids—A General Approach Toward Standardization", *IEEE Transactions on Industrial Electronics*, vol.58, no.1, pp.158-172, Jan. 2011.
- [6] C. L. Moreira, F. O. Resende, J. A. P. Lopes, "Using Low Voltage MicroGrids for Service Restoration," *IEEE Transactions on Power Systems*, vol.22, no.1, pp.395-403, Feb. 2007
- [7] F. Resende, N. Gil, J.A. Peças Lopes, "Service restoration on distribution systems using Multi-MicroGrids", *European Transactions on Electrical Power*, vol.21, no.2, pp.1327-1342, March 2011.
- [8] Thi Thu Ha Pham; Besanger, Y.; Hadjsaid, N.; , "New Challenges in Power System Restoration With Large Scale of Dispersed Generation Insertion," *IEEE Transactions on Power Systems*, vol.24, no.1, pp.398-406, Feb. 2009
- [9] M.M. Adibi, L.H. Fink, "Power system restoration planning," *IEEE Transactions on Power Systems*, vol.9, no.1, pp.22-28, Feb 1994.
- [10] T. D. Sudhakar, K. N. Srinivas, "Restoration of power network – a bibliographic survey", *European Transactions on Electrical Power*, vol. 21, no.1, pp. 635–655, January 2011.
- [11] M. Adibi, P. Clelland, L. Fink, H. Happ, R. Kafka, J. Raine, D. Scheurer, F. Trefny, "Power System Restoration - A Task Force Report," *IEEE Transactions on Power Systems*, vol.2, no.2, pp.271-277, May 1987.
- [12] J. A. Peças Lopes, Silvan A. Polenz, C.L. Moreira, Rachid Cherkaoui, "Identification of control and management strategies for LV unbalanced microgrids with plugged-in electric vehicles", *Electric Power Systems Research*, vol. 80, Issue 8, pp. 898-906, August 2010.
- [13] J. A. Peças Lopes, F.J. Soares, P.M.R. Almeida, "Integration of Electric Vehicles in the Electric Power System," *Proceedings of the IEEE*, vol.99, no.1, pp.168-183, Jan. 2011.
- [14] C. Gouveia, P. Ribeiro, C. L. Moreira, J. A. Peças Lopes, "Operational Characteristics of MicroGrids with Electric Vehicles", 12th International Conference on Probabilistic Methods Applied to Power Systems, Istanbul, 10-14th. June, 2012.
- [15] M. Savaghebi, A. Jalilian, J.C. Vasquez, J.M. Guerrero, "Autonomous Voltage Unbalance Compensation in an Islanded Droop-Controlled Microgrid," *IEEE Transactions on Industrial Electronics*, vol.60, no.4, pp.1390-1402, April 2013.
- [16] M. Savaghebi, A. Jalilian, J.C. Vasquez, J.M. Guerrero, "Secondary Control Scheme for Voltage Unbalance Compensation in an Islanded Droop-Controlled Microgrid," *IEEE Transactions on Smart Grid*, vol.3, no.2, pp.797-807, June 2012.
- [17] Y. Li, D. M. Vilathgamuwa, P. C. Loh, "Microgrid power quality enhancement using a three-phase four-wire grid-interfacing compensator." *IEEE Transactions on Industry Applications*, vol. 41, n. 6, pp. 1707-1719, November/December 2005.
- [18] F. Katiraei, M.R. Iravani, "Power Management Strategies for a Microgrid With Multiple Distributed Generation Units", *IEEE Transactions on Power Systems*, vol.21, no.4, pp.1821-1831, Nov. 2006
- [19] CENELEC EN 50160, "Voltage characteristics of electricity supplied by public distribution systems," November 1994.
- [20] Smart Grids with Electric Vehicles Laboratory [Online]: <http://reive.inescporto.pt/en/laboratory> (Last consulted on Feb. 2013).
- [21] SMA Report, "Technology Compendium 2-Solar Stand-Alone Power and Backup Power Supply", SMA 2009. (Available at: <http://files.sma.de/dl/10040/INSELVERSOR-AEN101410.pdf>)
- [22] R.J. Ferreira, L.M. Miranda, R.E. Araújo, J.P. Lopes, "A new bi-directional charger for vehicle-to-grid integration," 2011 2nd IEEE PES International Conference and Exhibition on Innovative Smart Grid Technologies (ISGT Europe), pp.1-5, 5-7 Dec. 2011.
- [23] M. Ciobotaru, R. Teodorescu, F. Blaabjerg, "A New Single-Phase PLL Structure Based on Second Order Generalized Integrator," *PESC '06. 37 the IEEE Power Electronics Specialists Conference*, pp.1,6, 18-22 June 2006, Jeju, South Korea.
- [24] R. Araújo Ferreira, R. Esteves Araújo, J. Peças Lopes, A comparative analysis and implementation of various PLL techniques applied to singlephase grids, *IYCE 2011 - 3rd International Youth Conference on Energeticas 2011*, Leiria, Julho, 2011.
- [25] M.N. Kheraluwala, R.W. Gascoigne, D.M. Divan, E.D. Baumann,, "Performance characterization of a high-power dual active bridge DC-to-DC converter," *Industry Applications, IEEE Transactions on*, vol.28, no.6, pp.1294,1301, Nov/Dec 1992.

## 9. Biographies

**Clara Gouveia** graduated in Electrical Engineering from the Faculty of Engineering, University of Porto FEUP (2008), and is currently working towards her PhD in Power Systems, also from the University of Porto. She is a member of the INESC-Porto research team and her research is focused on the development of the MicroGrid concept integrating plugged-in electrical vehicles in the operation of the electric system.

**Carlos Leal Moreira** received the B.S. and Ph.D. degrees in electrical engineering from the University of Porto, Porto, Portugal, in 2003 and 2008, respectively. Since 2010 he is the Smart Grid Area leader in the Power Systems Unit of the Institute for Systems and Computer Engineering of Porto (INESC Porto). He is also assistant professor in the Department of Electrical Engineering of the Faculty of Engineering of University of Porto since 2008. His main research interests are focused on microgrids dynamics and control, smart grids and smart metering.

**João Abel Peças Lopes (M'80–SM'94)** received the B.S. and Ph.D. degrees in electrical engineering from the University of Porto, Porto, Portugal, in 1981 and 1988. Since 2008, he is a full Professor of the Department of Electrical and Computer Engineering and is the Director of the Ph.D. Program on Sustainable Energy Systems, Faculty of Engineering, University of Porto. He is a Director of the Institute for Systems and Computer Engineering of Porto (INESC Porto), where he has been responsible for INESC Porto activities in several EU financed research projects. He is author or co-author of more than 200 papers.

**Diogo Varajão (S'12)** received the M.Sc. degree in electrical and computer engineering from the Faculty of Engineering, University of Porto (FEUP), Porto, Portugal, in 2012. During his master thesis he worked with matrix converters to develop a single-stage bidirectional electric vehicle charger with galvanic isolation. He is currently working toward his Ph.D. degree at FEUP and is with the Smart Grids with Electric Vehicles Laboratory of INESC Porto. He is a Student Member of the IEEE and a member of IES. He worked on the REIVE project in the development of power electronic converters for electric vehicles and microgeneration systems.

**Rui Esteves Araújo (M'99)** received the B.Sc. degree in electrical engineering and the M.Sc. and Ph.D. degrees from the University of Porto, Porto, Portugal, in 1987, 1992, and 2001, respectively. Since 1989, he has been with the University of Porto, where he is currently an Assistant Professor of the Department of Electrical and Computer Engineering, Faculty of Engineering, University of Porto. He is senior researcher in the INESC TEC, focusing on control theory and its industrial applications to motion control, electric vehicles and renewable energies. He coordinated the field of power electronics inside on the REIVE project.

© 2013 IEEE. Personal use of this material is permitted. Permission from IEEE must be obtained for all other uses, in any current or future media, including reprinting/republishing this material for advertising or promotional purposes, creating new collective works, for resale or redistribution to servers or lists, or reuse of any copyrighted component of this work in other works.



# Annex

## List of Figures

Fig. 1. Microgrid architecture integrating EV.....	24
Fig. 2. Centralized secondary control algorithm. ....	25
Fig. 3. Four-legg VSI with voltage balancing unit connected to the MG Main Storage unit.....	26
Fig. 4. EV control and interaction with the MGCC for the MG service restoration: a) general control diagram and b) frequency droop characteristic.....	27
Fig. 5. MG simulation case study. ....	28
Fig. 6. Synchronization of the SSMTs with the MG: a) MG and SSMT frequency b) main storage unit and SSMT active power). ....	29
Fig. 7. MG frequency response during system rebuilding. ....	30
Fig. 8. EV individual and total power output during MG rebuilding. ....	31
Fig. 9. Active power injected by the MG main storage unit. ....	32
Fig. 10. Negative and zero sequence voltage unbalance at the VSI terminals: a) considering the voltage balancing mechanisms and b) considering a common three-leg inverter .....	33
Fig. 11. VSI terminal voltage: a) considering the voltage balancing mechanisms and b) considering a common three-leg inverter. ....	34
Fig. 12. Negative and zero sequence voltage unbalance at Node 71: considering voltage balancing mechanisms. ....	35
Fig. 13. Node 71 voltage: a) considering the voltage balancing mechanisms and b) considering a common three-leg inverter. ....	36
Fig. 14. Architecture of the EV bidirectional charger prototype.....	37
Fig. 15. EV bidirectional charger prototype.....	38
Fig. 16. MG test system for testing the EV frequency support during Black Start. ....	39
Fig. 17. Load reconnection during BS procedure. ....	40
Fig. 18. MG frequency and EV power response during BS procedure.....	41
Fig. 19. MS reconnection and load variation. ....	42
Fig. 20. MG frequency and EV power response during load variation.....	43

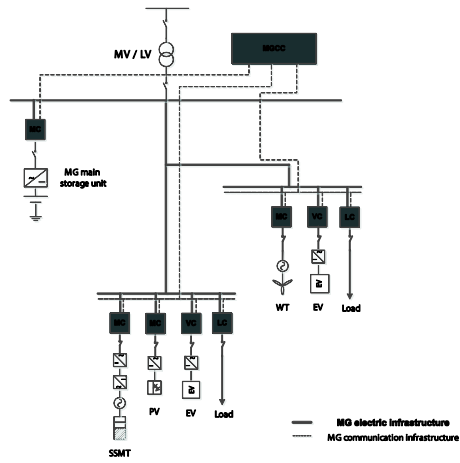


Fig. 1. Microgrid architecture integrating EV.

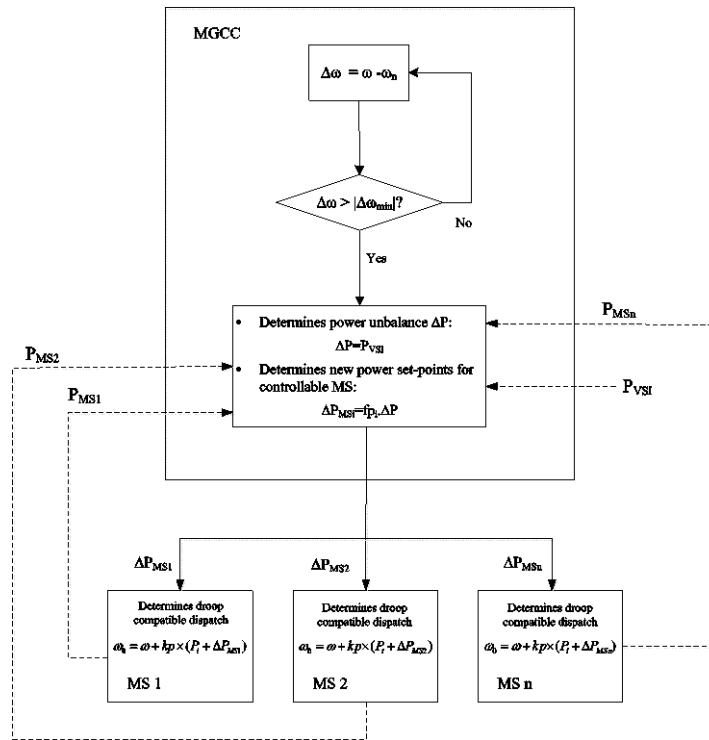


Fig. 2. Centralized secondary control algorithm.

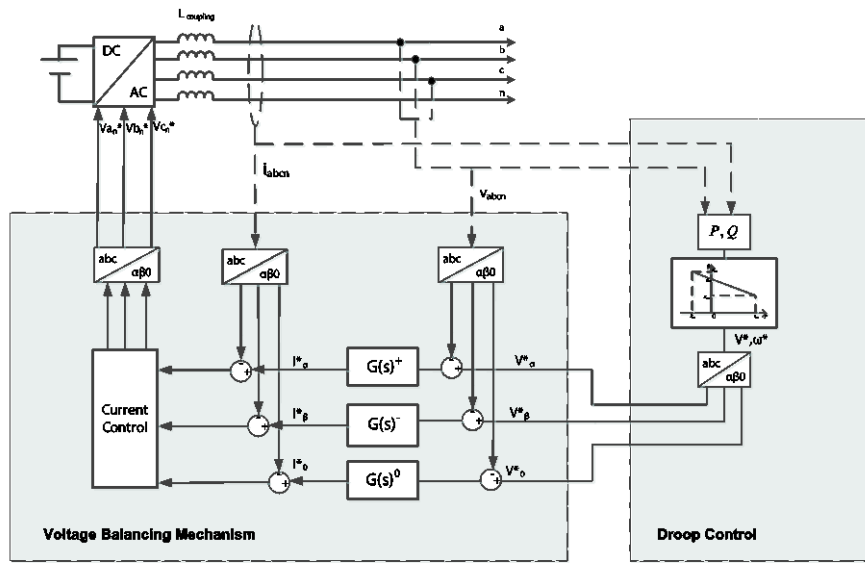


Fig. 3. Four-leg VSI with voltage balancing unit connected to the MG Main Storage unit.

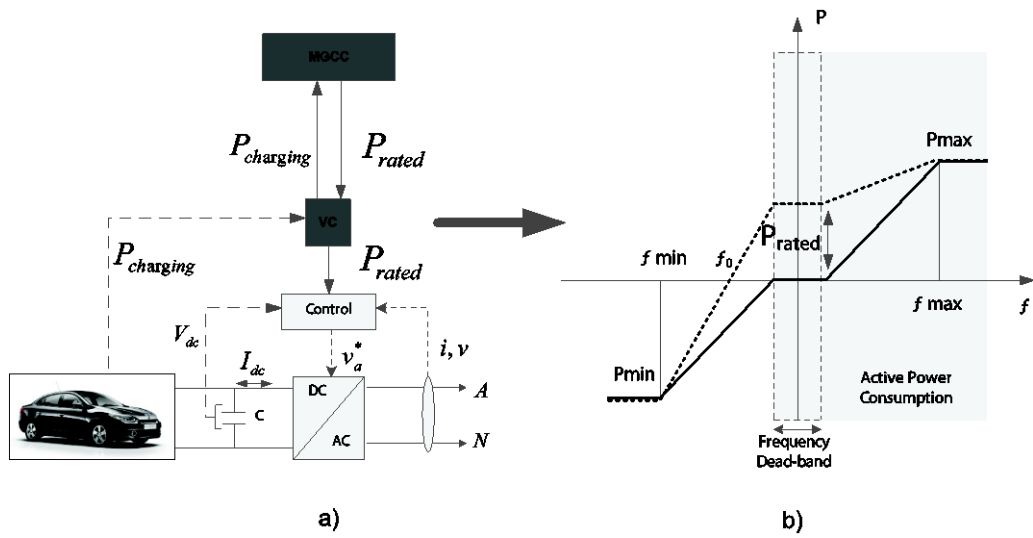


Fig. 4. EV control and interaction with the MGCC for the MG service restoration: a) general control diagram and b) frequency droop characteristic.

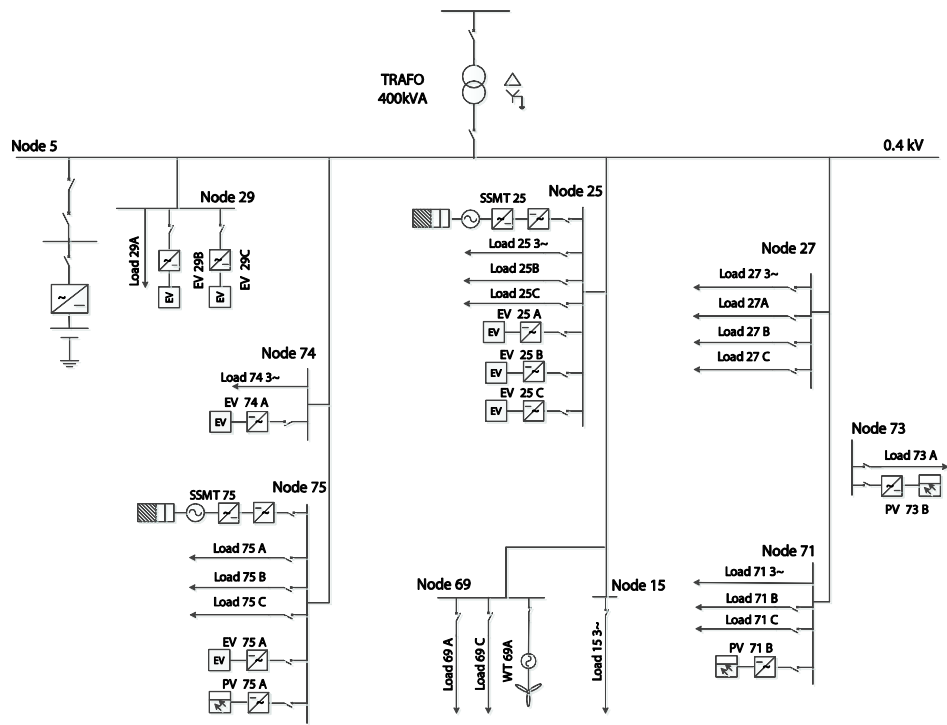
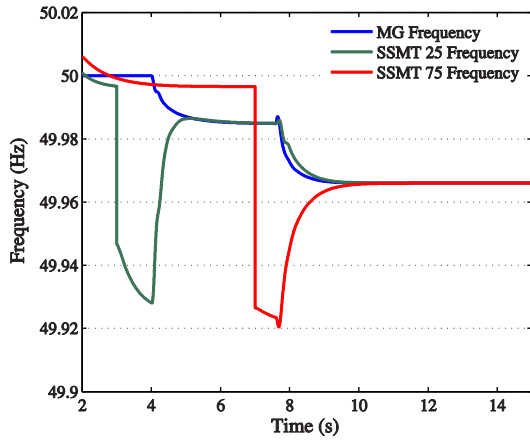
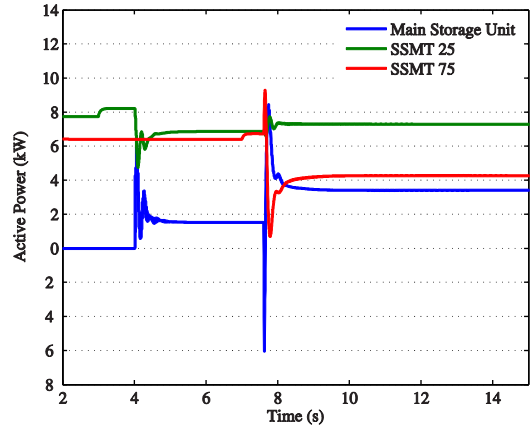


Fig. 5. MG simulation case study.



a)



b)

Fig. 6. Synchronization of the SSMTs with the MG: a) MG and SSMT frequency b) main storage unit and SSMT active power).

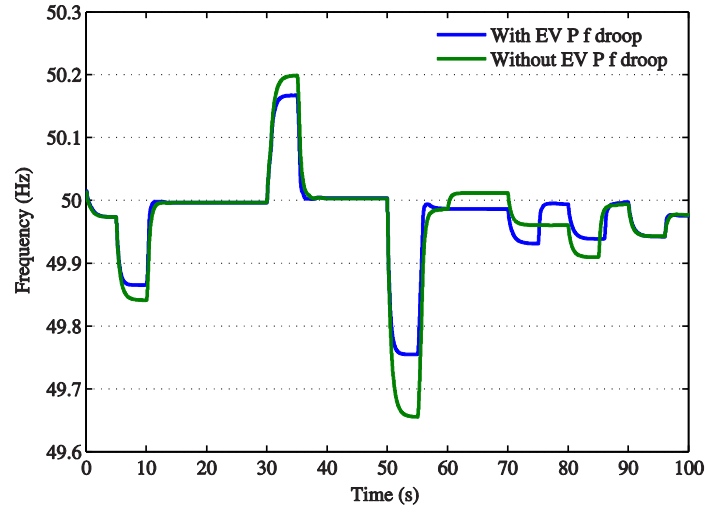


Fig. 7. MG frequency response during system rebuilding.

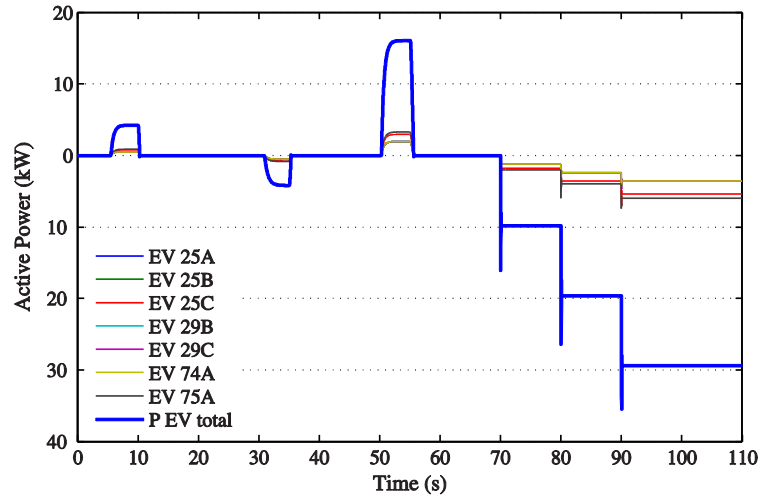


Fig. 8. EV individual and total power output during MG rebuilding.

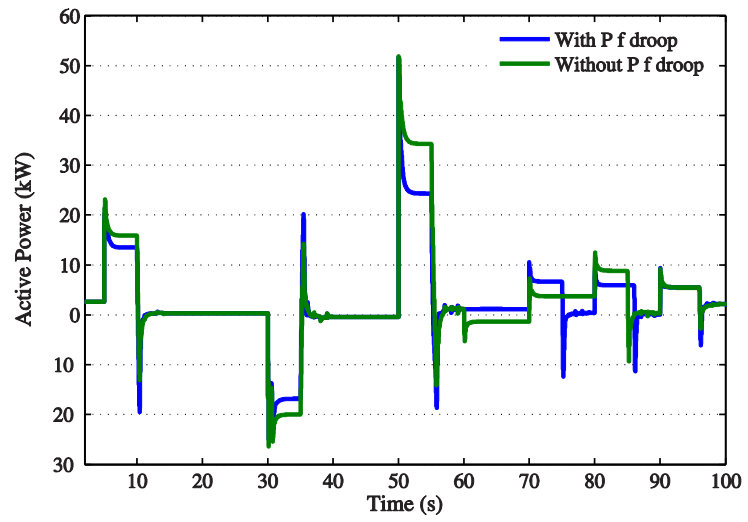


Fig. 9. Active power injected by the MG main storage unit.

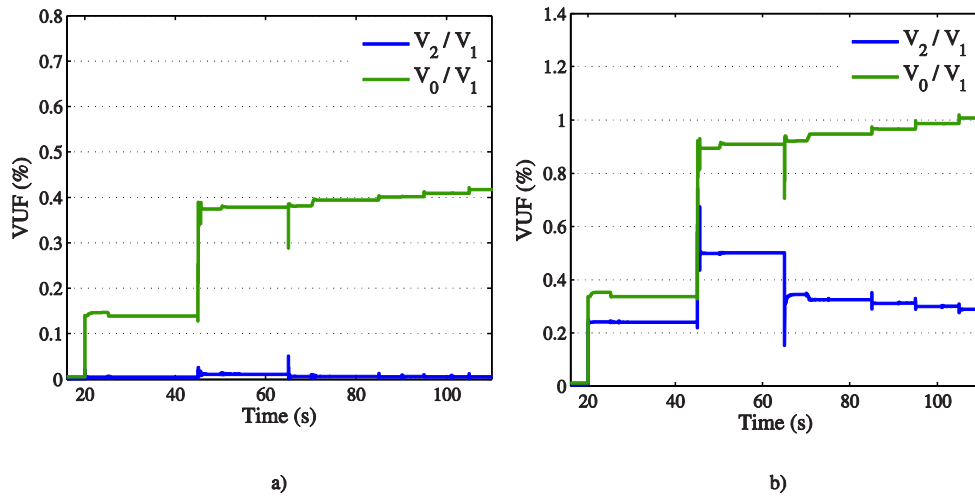


Fig. 10. Negative and zero sequence voltage unbalance at the VSI terminals: a) considering the voltage balancing mechanisms and b) considering a common three-leg inverter

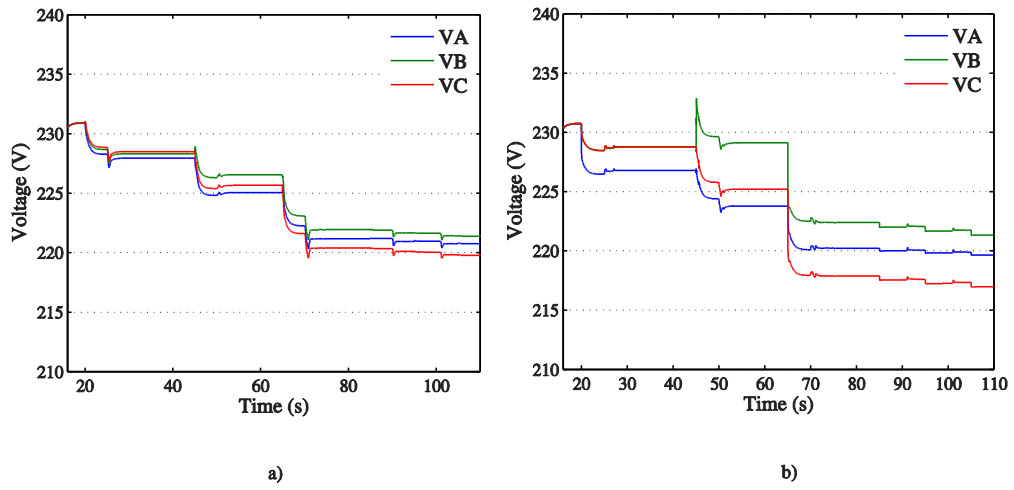


Fig. 11. VSI terminal voltage: a) considering the voltage balancing mechanisms and b) considering a common three-leg inverter.

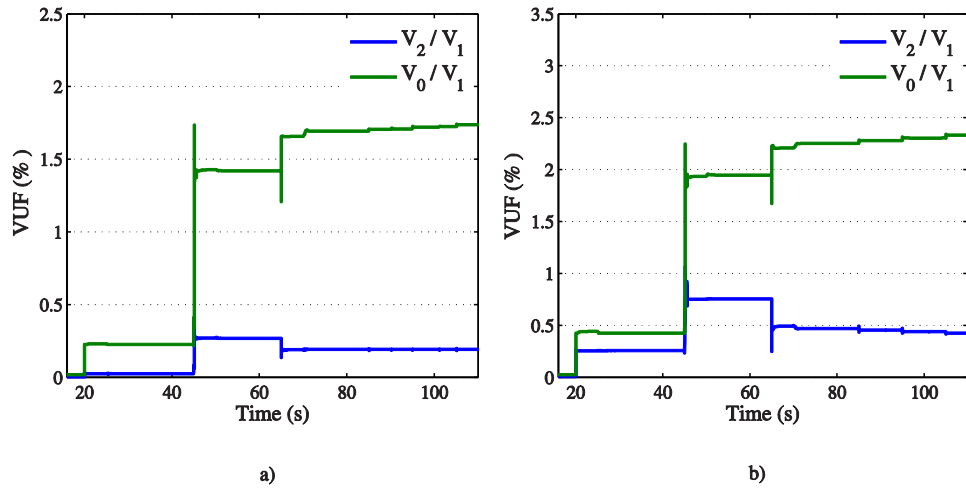
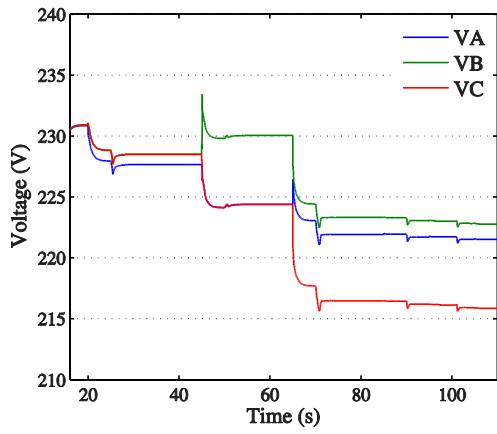
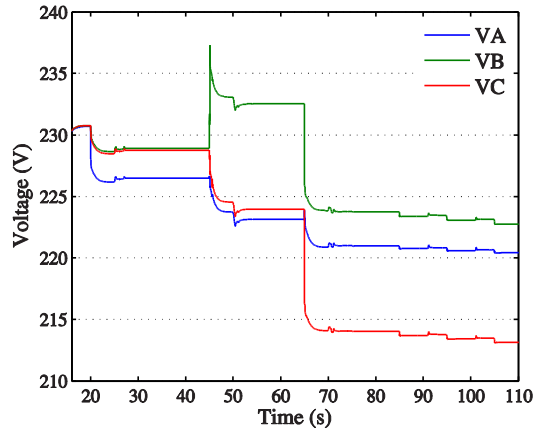


Fig. 12. Negative and zero sequence voltage unbalance at Node 71: considering voltage balancing mechanisms.



a)



b)

Fig. 13. Node 71 voltage: a) considering the voltage balancing mechanisms and b) considering a common three-leg inverter.

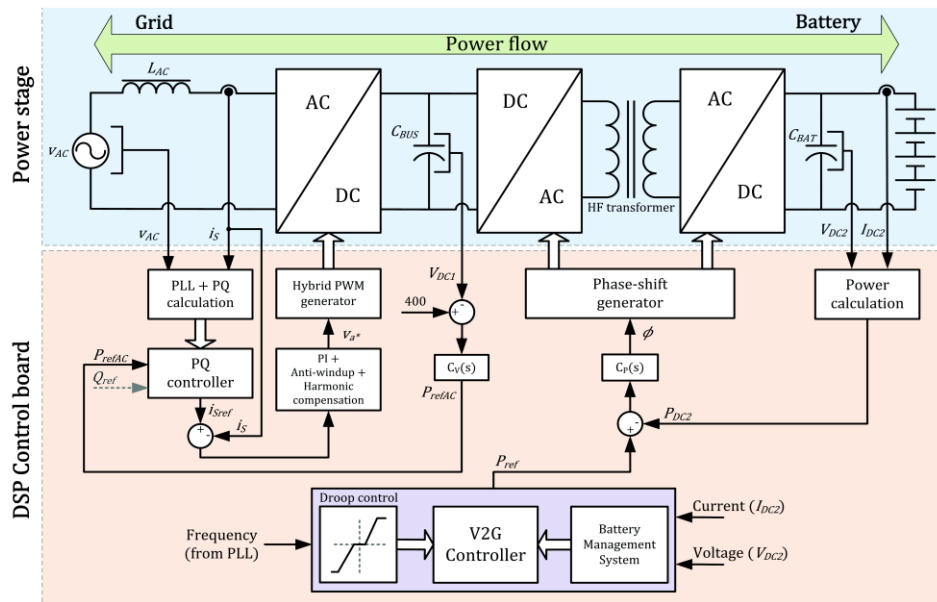
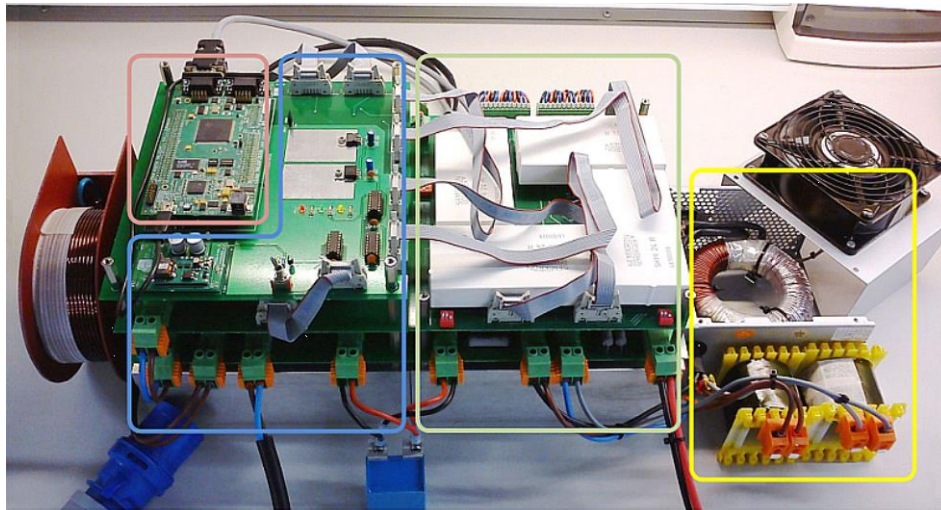


Fig. 14. Architecture of the EV bidirectional charger prototype.



DSP Control Board Full-Bridge Inverter Dual Active Bridge HF Transformer

Fig. 15. EV bidirectional charger prototype.

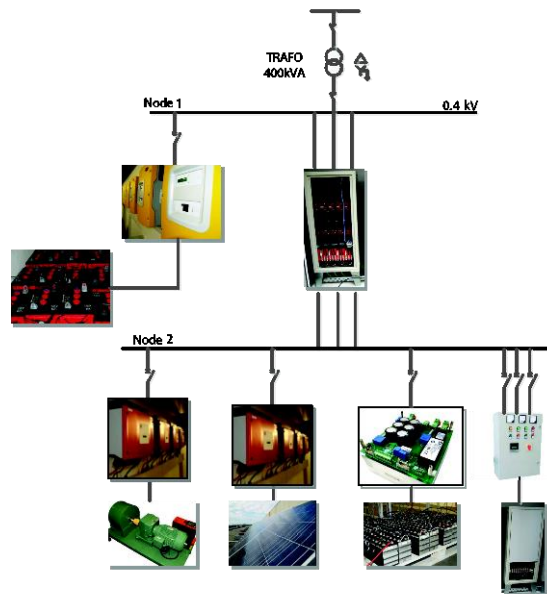


Fig. 16. MG test system for testing the EV frequency support during Black Start.

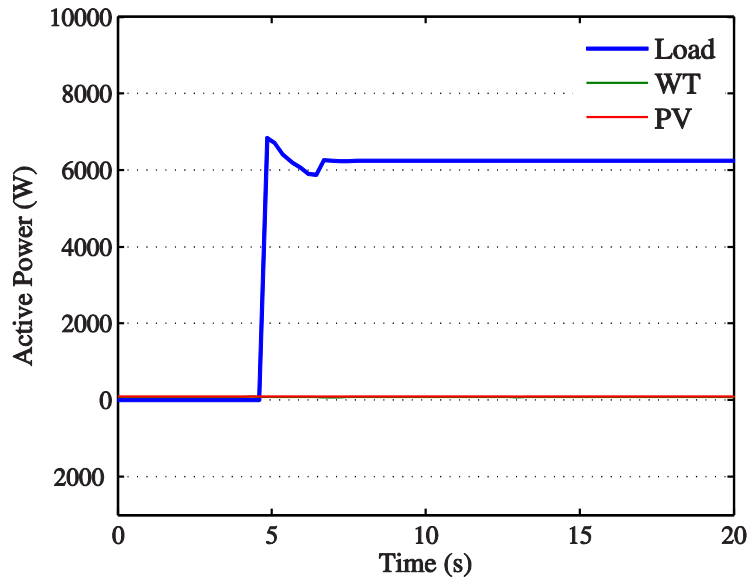


Fig. 17. Load reconnection during BS procedure.

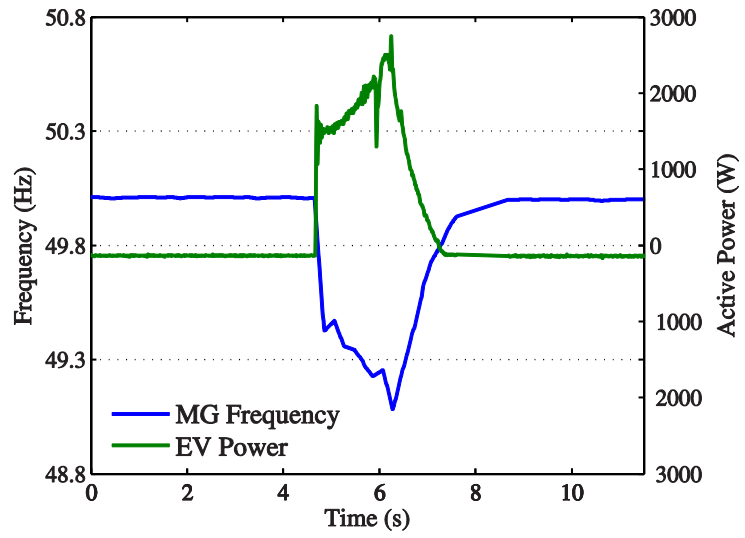


Fig. 18. MG frequency and EV power response during BS procedure.

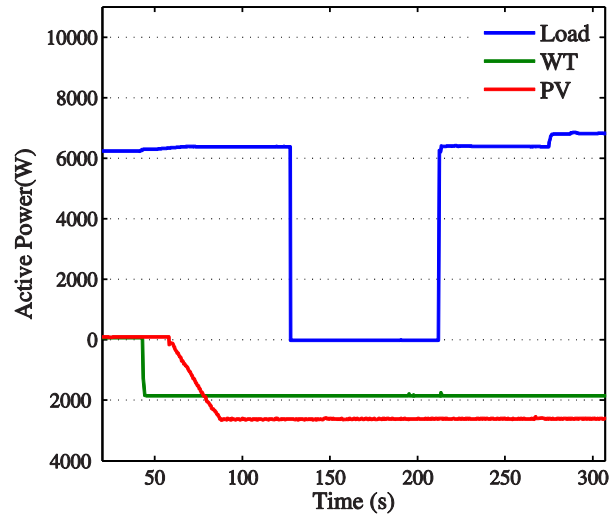


Fig. 19. MS reconnection and load variation.

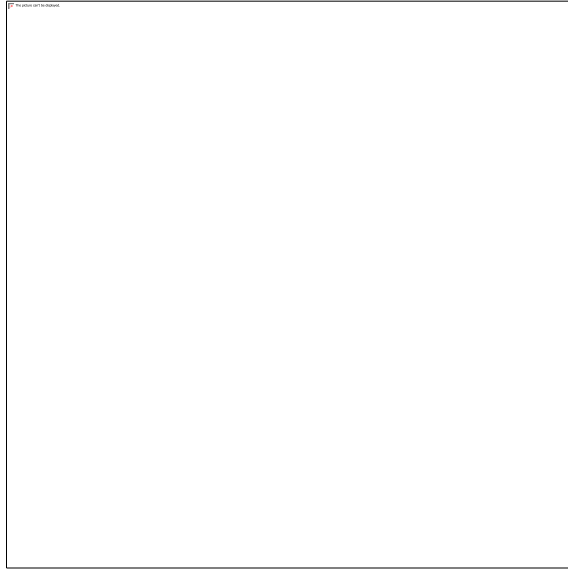


Fig. 20. MG frequency and EV power response during load variation.

List of Tables

Table I – MG simulation scenario summary .....45

Table II – Simulated procedure for the MG service restoration.....46

Table I – MG simulation scenario summary.

	Three-Phase	Single-Phase			Total
		A	B	C	
<b>Load (kW)</b>	42	20	25	33	120
<b>EV (kW)</b>	-	22	12	15	49
<b>PV (kW)</b>	-	0	16	12	28
<b>WT (kW)</b>	-	8	0	0	8
<b>SSMT 25 (kW)</b>	30	-	-	-	30
<b>SSMT 75 (kW)</b>	60				60

Table II – Simulated procedure for the MG service restoration.

**MG rebuilding:**

**1. Synchronization of the SSMT to the MG:**

(a)  $t=3s$  – MGCC enables the synchronization of SSMT25.

(b)  $t=7s$  – MGCC enables the synchronization of SSMT75.

**2. Connection of EV with zero charging power ( $t=16s$ ).**

**3. Reconnection of loads and MS:**

(c)  $t=20s$  – Reconnection of the first load group (Total load of 24.4 kW - loads connected to nodes 15, 29, 73, 74, 75).

(d)  $t=45s$  Reconnection of non-controllable MS (Total of 36 kW: 69, 71, 73 and 75).

(e)  $t=65s$ - Reconnection of the second loads group (Total load of 60.3 kW: 27, 69, 71).

(f) Increase of EV charging power, by changing the  $P_{rated}$  droop parameters:

–  $t=85s$  – EV  $P_{rated}$  is increased from 0 to 20%  $P_{nom}$

–  $t=95s$  - EV  $P_{rated}$  is increased to 40%  $P_{nom}$

–  $t=105s$  - EV  $P_{rated}$  is increased to 60%  $P_{nom}$

**4. Synchronization and reconnection to the MV Grid.**

List of Equations

Equation 1 .....	48
Equation 2 .....	49

$$\begin{aligned}\omega &= \omega_0 - k_p \times (P_i + \Delta P) \\ V &= V_0 - k_Q \times (Q_i + \Delta Q)\end{aligned}\quad (1)$$

$$\begin{bmatrix} 1 & k_{P_1} & 0 & \cdots & 0 \\ 1 & 0 & k_{P_2} & \cdots & 0 \\ \cdots & \cdots & \cdots & \ddots & \vdots \\ 1 & 0 & 0 & \cdots & k_{P_n} \\ 0 & 1 & 1 & \cdots & 1 \end{bmatrix} \times \begin{bmatrix} \omega' \\ (P_{i_1} + \Delta P_1) \\ (P_{i_2} + \Delta P_2) \\ \vdots \\ (P_{i_n} + \Delta P_n) \end{bmatrix} = \begin{bmatrix} \omega_{01} \\ \omega_{02} \\ \vdots \\ \omega_{0n} \\ \Delta P \end{bmatrix} \quad (2)$$